Electron impact ionization dynamics of para-benzoquinone

D. B. Jones, E. Ali, C. G. Ning, J. Colgan, O. Ingólfsson, D. H. Madison, and M. J. Brunger

Citation: The Journal of Chemical Physics **145**, 164306 (2016);
View online: https://doi.org/10.1063/1.4965919
View Table of Contents: http://aip.scitation.org/toc/jcp/145/16
Published by the American Institute of Physics

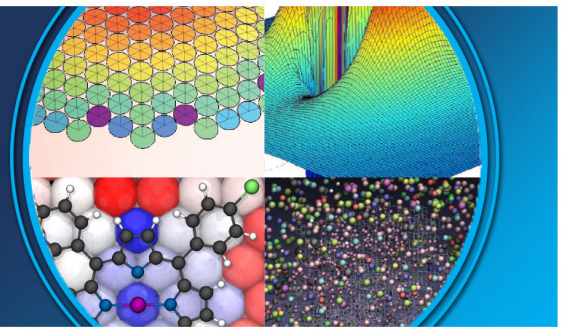

Electron impact ionization dynamics of *para*-benzoquinone

D. B. Jones,[1,a)] E. Ali,[2] C. G. Ning,[3] J. Colgan,[4] O. Ingólfsson,[5] D. H. Madison,[2] and M. J. Brunger[1,6,a)]

[1]*School of Chemical and Physical Sciences, Flinders University, GPO Box 2100, Adelaide SA 5001, Australia*
[2]*Department of Physics, Missouri University of Science and Technology, Rolla, Missouri 65409, USA*
[3]*Department of Physics, State Key Laboratory of Low-Dimensional Quantum Physics, Tsinghua University, Beijing 100084, China*
[4]*Theoretical Division, Los Alamos National Laboratory, Los Alamos, New Mexico 87545, USA*
[5]*Science Institute and Department of Chemistry, University of Iceland, Dunhagi 3, 107 Reykjavík, Iceland*
[6]*Institute of Mathematical Sciences, University of Malaya, 50603 Kuala Lumpur, Malaysia*

(Received 4 September 2016; accepted 10 October 2016; published online 27 October 2016)

Triple differential cross sections (TDCSs) for the electron impact ionization of the unresolved combination of the 4 highest occupied molecular orbitals ($4b_{3g}$, $5b_{2u}$, $1b_{1g}$, and $2b_{3u}$) of *para*-benzoquinone are reported. These were obtained in an asymmetric coplanar geometry with the scattered electron being observed at the angles −7.5°, −10.0°, −12.5° and −15.0°. The experimental cross sections are compared to theoretical calculations performed at the molecular 3-body distorted wave level, with a marginal level of agreement between them being found. The character of the ionized orbitals, through calculated momentum profiles, provides some qualitative interpretation for the measured angular distributions of the TDCS. *Published by AIP Publishing.* [http://dx.doi.org/10.1063/1.4965919]

I. INTRODUCTION

Oxygenic photosynthesis is the principle energy converter on earth,[1] converting H_2O and CO_2 into sugars and O_2. An understanding of the individual processes within the photosynthetic cycle thus has broad implications for technological development. Specifically, it is desirable to increase the light capturing efficiency and to identify and then remove competitive chemical pathways that offer less efficient oxygenation reactions.[2] This has the potential to improve biomass generation, which may in turn increase the viability of a sustainable biofuel industry. Enhancing our understanding of naturally occurring photosynthesis may also drive innovation in photovoltaics and photocatalysis,[3] and also the creation of hybrid photo-bioelectrochemical technologies.[4] Quinones play a particularly important role in photochemical systems through their ability to undergo reversible reduction (i.e., from plastoquinone to plastoquinol). The ability to undergo reversible reduction also makes quinones an important substance within the electron transport chain of cellular respiration. The unique electrochemical properties of quinones have further enabled their use as a low-cost and sustainable material for energy storage applications.[5,6]

para-Benzoquinone (2,5-cyclohexadiene-1,4-dione, $C_6H_4O_2$, see Figure 1), hereafter referred to as pBQ, is the simplest quinone. It has therefore served as a prototypical structure in a number of studies aiming to understand the photo-induced and electrochemical behaviours of quinones in general. Correspondingly, the structures of its ground, excited, anionic, and cationic states,[7–10] as well as that of its derivatives[11] and complexes[12] have attracted significant theoretical attention over an extended period of time. There has also been extensive experimental studies into the photodynamics of pBQ[8,13–16] and the bulk of the spectroscopic and theoretical studies conducted have been reviewed by Itoh in 1995,[17] and a fairly comprehensive literature overview is given in Ómarsson and Ingólfsson.[18] From an electron scattering perspective, however, it is only vibrational and electronic excitation,[19] negative ion formation, and the resonances[18,20–26] of pBQ and its derivatives that have been investigated. The cationic forms of pBQ and its derivatives have also been investigated experimentally through photoionization,[27–30] Penning ionization,[31] and matrix isolation spectroscopy.[32] The interpretation of the cationic structure of pBQ has, however, been controversial as vibronic coupling occurs between the outermost orbitals that lie close in energy,[32] while there is also a strong influence of electron correlation in the cationic states.[11] Further knowledge of the cationic structure and the ionization dynamics of pBQ is therefore important in understanding chemical reactivity within the quinone family of compounds.

In this paper, we present a combined experimental and theoretical investigation into electron impact ionization of the unresolved combination of the four highest occupied molecular orbitals ($4b_{3g}$, $5b_{2u}$, $1b_{1g}$, and $2b_{3u}$) of pBQ. Here we employed an (e,2e) coincident technique using the asymmetric coplanar kinematics depicted in Fig. 2, with an intermediate impact energy (E_0). This kinematically complete electron impact ionization process is described through

$$e_0^-(E_0,\boldsymbol{k}_0) + \mathrm{pBQ} \rightarrow \mathrm{pBQ}^+(\epsilon_i) + e_1^-(E_1,\boldsymbol{k}_1) + e_2^-(E_2,\boldsymbol{k}_2)\,. \quad (1)$$

a)Authors to whom correspondence should be addressed. Electronic addresses: darryl.jones@flinders.edu.au and michael.brunger@flinders.edu.au

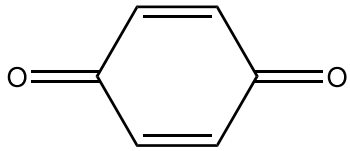

FIG. 1. Schematic representation of *para*-benzoquinone (pBQ, 1,4-benzoquinone).

Here E_j and $\boldsymbol{k}_j$ ($j = 0$, 1, or 2) are the energies and momenta of the incident, fast-scattered, and slow-ejected electrons, respectively. The conservation of energy requires that

$$\epsilon_i = E_0 - (E_1 + E_2), \tag{2}$$

where ϵ_i is the energy required to ionize the ith-orbital of pBQ. The ion created recoils from the collision with momentum,

$$\boldsymbol{q} = \boldsymbol{k}_0 - (\boldsymbol{k}_1 + \boldsymbol{k}_2). \tag{3}$$

Angular distributions of the triple differential cross section for the ejected electron were obtained when the faster electron was scattered through a fixed angle of either $\theta_1 = -7.5°$, $-10.0°$, $-12.5°$ or $-15.0°$. Under these conditions, a change to the fixed scattered electron angle reflects a change in the momentum transferred ($\boldsymbol{K} = \boldsymbol{k}_0 - \boldsymbol{k}_1$) to the molecule during the ionization process. Such conditions are important for establishing a link between high impact ionization phenomena that can probe the internal structure of molecules,[33–35] and low impact energy collisions that investigate the collision dynamics.[36] These kinematical conditions are also similar to those employed in our previous investigations on the ionization dynamics of larger molecules.[37–43] Further, our current experimental investigations relate to the ionization dynamics of biologically relevant molecular targets that contain oxygen atoms in varying chemical environments.[40–43] In this way, we can experimentally assess the role of the oxygen atom's bonding network and its proximity to the surrounding functional groups in the collisional dynamics. In the current contribution, we chose to study the angular distributions of the triple differential cross section (TDCS) over a finely spaced range of scattered electron angles in order to investigate how rapidly the TDCS varies. This was prompted by recent experimental and theoretical investigations into the electron impact ionization of argon, under comparable intermediate energy asymmetric kinematic conditions.[44–46] Those argon studies revealed that the magnitude of the TDCS changed rapidly with the scattered electron angle. We therefore wished to evaluate how the magnitude of the TDCS varied as a function of the scattered electron angle for a more complicated, molecular target.

The final, more general point we wish to make is that the present and like-minded investigations are important for the development of models of electron transport in matter. One such model, the low-energy particle track simulation (LEPTS) code from Garcia and colleagues,[47–50] currently describes the ionization process through the total ionization cross section and empirical double differential cross sections (derived from average energy-loss distributions and elastic scattering angular distributions), with the ejected secondary electron moving off in the direction of the momentum transfer (+K) vector.[51] In effect, this neglects all considerations of the shape of the TDCS in the binary region, and discounts the possibility of recoil scattering. The present study, and our earlier studies,[37–43] which includes work on bio-molecules, explicitly investigates the angular distribution of the TDCS under different kinematical conditions, and so directly probes the validity of the ionization model currently used by Garcia and his co-workers.[47–50]

The outline of the remainder of our paper is as follows: In Section II, the details of our experimental and theoretical methods are summarised. We then present and discuss our results in Section III. Finally, in Section IV, some conclusions are drawn from this investigation.

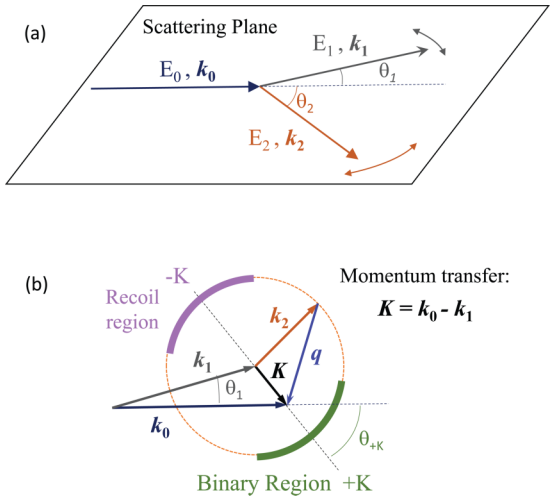

FIG. 2. (a) Schematic representation of the asymmetric coplanar kinematics used in the present measurements for electron impact ionization of pBQ. (b) A diagrammatic representation of the momentum transferred to the target ($\boldsymbol{K}$) and the conservation of momentum within the present asymmetric coplanar kinematics. Here $\boldsymbol{q}$ represents the recoil momentum of the residual ion. The binary and recoil regions represent the angular ranges where the ejected electron (having momentum $\boldsymbol{k_2}$) leaves the collision in the directions close to parallel and antiparallel to the momentum transfer direction (θ_{+K}), respectively. See text for further details.

II. EXPERIMENTAL AND THEORETICAL DETAILS

Triple differential cross sections for the electron impact ionization of pBQ have been measured using an electron-electron coincidence technique. The details of the (e,2e) coincidence spectrometer have been described previously in Cavanagh and Lohmann.[52] In brief, an electron beam intersects an effusive beam of pBQ with scattered and ejected electrons being detected using energy selective analysers that are mounted on independently rotatable turntables. The pBQ beam is produced from *para*-benzoquinone (98% assay, Sigma-Aldrich) that was degassed prior to use. *para*-Benzoquinone is a solid at room temperature that readily sublimes at reduced pressure. Its vapour pressure is, however, relatively low for collision studies (0.1 mm Hg at 25 °C) and we found pBQ to be a particularly challenging target for us to investigate experimentally. In this study, our most stable

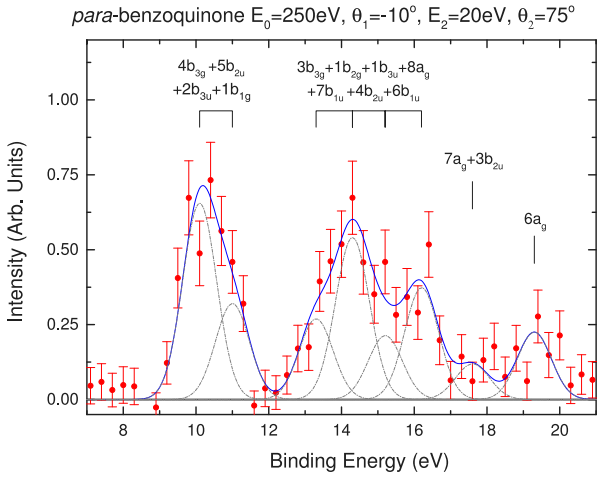

FIG. 3. The (e,2e) binding energy spectrum of *para*-benzoquinone obtained using an incident electron energy of 250 eV. The scattered electron energy was scanned for a fixed angle of detection, $\theta_1 = -10.0°$, while the ejected electron energy was detected at $\theta_2 = 75°$ with an energy of 20 eV. See text for further details.

experimental conditions were achieved when the gas handling lines and the scattering chamber were heated to 40 °C, with the pBQ sample being heated to ∼30 °C. Heating the sample to higher temperatures resulted in recrystallization within the inlet system, ultimately causing a blockage in our sample handling system. Under our optimal running conditions, the experiments were conducted with a gauge-corrected chamber pressure of $\sim 9 \times 10^{-7}$ Torr.

An electron impact ionization binding energy spectrum for pBQ was first obtained by recording the number of true coincident electron impact ionization events while repeatedly scanning over a range of scattered electron energies. Here the incident and ejected electron energies were fixed at 250 eV and 20 eV, respectively. For these measurements, both the scattered and ejected electron analyser positions were fixed at −10.0° and 75.0°, respectively. A typical example of a pBQ binding energy spectrum from the present electron impact ionization investigation is given in Figure 3. Angular distributions of the electron impact ionization triple differential cross section are obtained by fixing the scattered electron analyser position (in this case at −7.5°, −10.0°, −12.5° or −15.0°), and scanning over a range of ejected electron angles. Here the incident and ejected electron energies are again fixed at 250 eV and 20 eV, respectively, while the scattered electron energy is fixed to investigate the unresolved combination of the 4 highest occupied molecular orbitals (see Figure 3). As our coincidence energy resolution is ∼1.1 eV (FWHM), the fixed scattered electron energy for the angular distribution measurements was taken to be the centre of the band for the $4b_{3g} + 5b_{2u} + 1b_{1g} + 2b_{3u}$ orbitals ($E_1 \sim 219.5$ eV). With all four of the outermost orbitals lying within 1 eV of energy, we believe that all orbitals should contribute equally within the experimental TDCS angular distribution measurement. The measured triple differential cross sections angular distributions for different scattered electron angles were then inter-normalised by fixing the ejected electron detector at 90° and measuring the TDCS while scanning over the range of scattered electron angles examined. The present experimental angular distributions are shown in Figure 4.

In order to interpret our measured spectra, quantum chemical calculations were performed in Gaussian 09.[53]

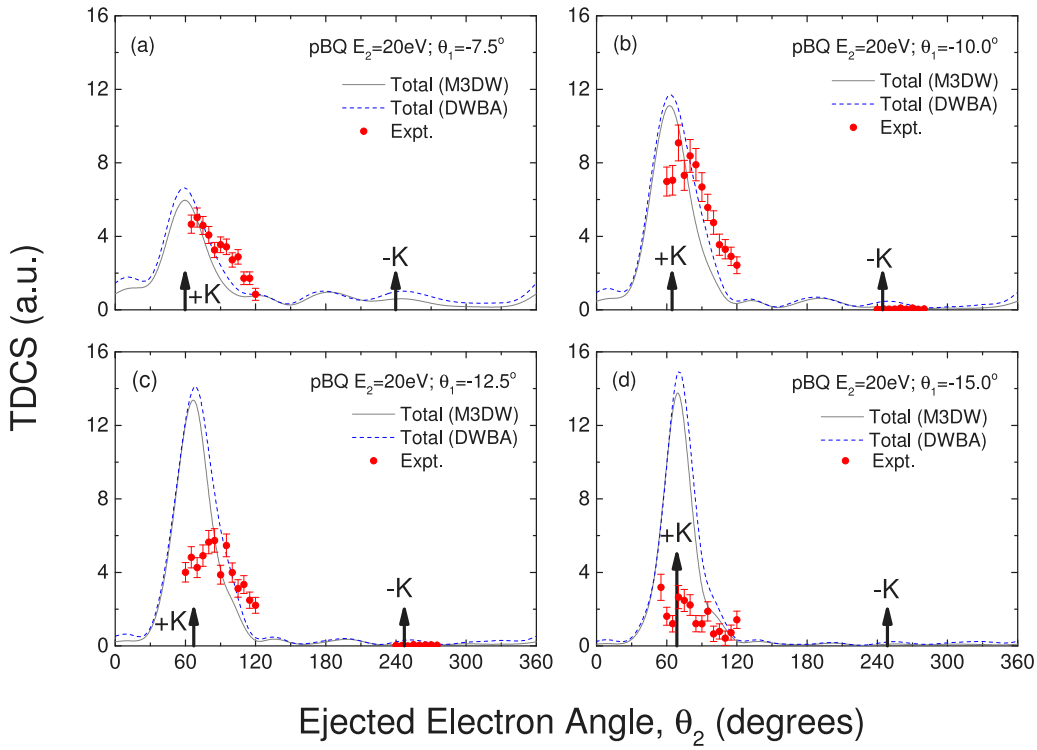

FIG. 4. Experimental and theoretical triple differential cross sections for the electron impact ionization of the unresolved combination of the $4b_{3g} + 5b_{2u} + 1b_{1g} + 2b_{3u}$ orbitals of pBQ for (a) $\theta_1 = -7.5°$, (b) $\theta_1 = -10.0°$, (c) $\theta_1 = -12.5°$, and (d) $\theta_1 = -15.0°$. Here the incident electron energy is 250 eV and the ejected electron energy is 20 eV. See text for further details. Note here that a.u. represents atomic units.

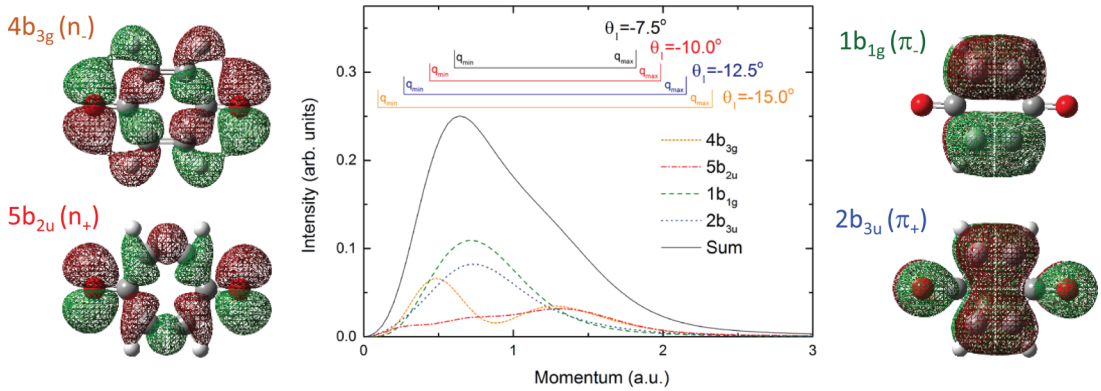

FIG. 5. Theoretical spatial orbital representation and momentum profiles of the pBQ orbitals we examined experimentally. Here the range of linear momenta examined under each kinematical condition is also depicted on the momentum profile. The summed momentum profile for the contributing orbitals is also presented. See text for further details.

The pBQ geometry was first optimised at the B3LYP/aug-cc-pVDZ level of theory, with the optimum geometry being in excellent accord with previously reported experimental and theoretical values that have been summarised in Ref. 10. The optimized geometry was then used for subsequent calculations performed at the B3LYP/aug-cc-pVDZ and OVGF/aug-cc-pVDZ levels of theory. As the pBQ electronic structure has been extensively studied using sophisticated methods,[7,11] our calculations were primarily done to assist us further in interpreting our measurements. We do note that we achieved excellent agreement with previous calculations performed at a similar level of theory.[11] The B3LYP/aug-cc-pVDZ calculations are used here to visualise the ionized orbitals and to obtain spherically averaged orbital momentum profiles through the HEMS program.[54] The spatial orbital representations and momentum profiles can be found in Figure 5.

To calculate triple differential cross sections (TDCSs) for the electron impact ionization of pBQ, we used the molecular three-body distorted wave (M3DW) approximation. This approach has been described elsewhere,[55,56] so we only provide a short overview here. The TDCS within the M3DW framework is given by

$$\frac{d^5\sigma}{d\Omega_1 d\Omega_2 dE} = \frac{1}{(2\pi)^5}\frac{k_1 k_2}{k_0}\left(|T_{dir}|^2 + |T_{exc}|^2 + |T_{dir} - T_{exc}|^2\right). \tag{4}$$

As before $\boldsymbol{k}_0$, $\boldsymbol{k}_1$ and $\boldsymbol{k}_2$ are the wave vectors for the initial, scattered, and ejected electrons, respectively. T_{dir} is the direct scattering amplitude, and T_{exc} is the exchange amplitude. The direct scattering amplitude is given by

$$T_{dir} = \left\langle \chi_1^-(\boldsymbol{k}_1,\boldsymbol{r}_0)\,\chi_2^-(\boldsymbol{k}_2,\boldsymbol{r}_1)\,C_{12}(\boldsymbol{r}_{01})\middle|V_0 - U_0|\phi_{Dy}(\boldsymbol{r}_1)\,\chi_0^+(\boldsymbol{k}_0,\boldsymbol{r}_0)\right\rangle, \tag{5}$$

where $\chi_0^+(\boldsymbol{k}_0,\boldsymbol{r}_0)$ is a continuum-state distorted wave for an incident electron with wave number $\boldsymbol{k}_0$ and the (+) indicates outgoing wave boundary conditions. Further, $\chi_1^-(\boldsymbol{k}_1,\boldsymbol{r}_0)$ and $\chi_2^-(\boldsymbol{k}_2,\boldsymbol{r}_1)$ are the scattered and ejected electron distorted waves with incoming wave boundary conditions. The factor $C_{12}(\boldsymbol{r}_{01})$ is the final state Coulomb-distortion factor between the two outgoing electrons—normally called the post collision interaction (PCI), and $\phi_{Dy}(\boldsymbol{r}_1)$ is the one-electron Dyson orbital averaged over all molecular orientations.[55] Calculations at the distorted wave Born approximation (DWBA) level, where we do not include the post collision interaction term, were also carried out.

III. RESULTS AND DISCUSSION

A typical binding energy spectrum for electron impact ionization of pBQ is presented in Figure 3. To assist in the interpretation of this spectrum, our calculated ionization energies and a summary of previous experimental photoelectron spectroscopy (PES) data are given in Table I. In Figure 3, we see a strong band for the unresolved combination of the 4 highest occupied molecular orbitals ($4b_{3g}$, $5b_{2u}$, $1b_{1g}$, and $2b_{3u}$). These orbitals have traditionally been described as symmetric and asymmetric non-bonding oxygen 2p orbitals [$4b_{3g}$ (n_-), $5b_{2u}$ (n_+)] and the out of plane π–ring bonding contributions [$1b_{1g}$ (π), $2b_{3u}$ (π)]. It is important to note that these 4-highest occupied orbitals are well separated from other molecular orbitals in pBQ, and they therefore form the subject of our ionization dynamics investigation.

Angular distributions for the triple differential cross sections for the unresolved combination of the four outermost orbitals are shown in Figure 4. These were measured for an incident electron energy of 250 eV and when the scattered electron was detected at $\theta_1 = -7.5°$, $-10.0°$, $-12.5°$ or $-15.0°$. Experimental angular distribution was observed in the binary and recoil regions, where the ejected electron leaves

TABLE I. Present (e,2e) and previous photoelectron spectroscopy (PES) experimental ionization potentials and presently calculated theoretical ionization potentials of pBQ (*para*-benzoquinone). See text for further details.

	PES[7,29]	PES[30]	PES[27]	PES[28]	OVGF/aug-cc-pVDZ		
Present (e,2e) Energy (eV)	Energy (eV)	Energy (eV)	Energy (eV)	Energy (eV)	IP (eV)	Pole strength	Assignment
10.1	10.11	9.99	9.99	10.05	10.36	0.888	$(4b_{3g})^{-1}$ [n$_-$]
	10.40	10.29	10.29	10.33	10.78	0.877	$(5b_{2u})^{-1}$ [n$_+$]
11.0	11.06	10.93	10.93	11.08	10.89	0.887	$(2b_{3u})^{-1}$ [π_+]
	11.5	11.0	11.1	11.08	10.90	0.903	$(1b_{1g})^{-1}$ [π_-]
13.3	13.4	13.5			14.08	0.877	$(3b_{3g})^{-1}$
	13.4				14.12	0.831	$(1b_{2g})^{-1}$
14.3	14.3	14.3			14.68	0.892	$(8a_g)^{-1}$
	14.8	14.9/15.0			15.05	0.847	$(1b_{3u})^{-1}$
15.2	14.7	14.8			15.26	0.885	$(7b_{1u})^{-1}$
	15.3	15.5			15.62	0.879	$(4b_{2u})^{-1}$
16.2	16.2	16.2/16.7			16.74	0.867	$(6b_{1u})^{-1}$
17.6	17.0	17.0			17.04	0.867	$(3b_{2u})^{-1}$
					17.29	0.861	$(7a_g)^{-1}$
19.3	19.5	19.5					

the collision in a direction that is close to parallel and anti-parallel with the momentum transfer direction, respectively. We note that we did attempt to measure the TDCSs in the recoil regions at $\theta_1 = -7.5°$ and $-15.0°$ but we could not achieve acceptable statistics for those angular distributions. This suggests that the TDCSs in the recoil regions for $\theta_1 = -7.5°$ and $-15.0°$ are particularly small. Even for the TDCSs at $\theta_1 = -10.0°$ and $-12.5°$, for which we were able to obtain acceptable true coincident signals in the recoil region, the uncertainties were of the order of ∼45%. To provide the reader with further clarity of the difficulties associated with these (e,2e) measurements, we note that our TDCS angular distribution data were obtained in an experimental runtime of ∼6 months. In order to compare with our theoretical results, the experimental data were normalised to the M3DW at a single point ($\theta_2 = 70°$) in the binary region of the $\theta_1 = -7.5°$ angular distribution. This single normalisation factor has been applied to the experimental data measured across all of the scattered electron angles. We now discuss and compare the experimental and theoretical TDCS data in more detail.

We begin with discussions of the binary peak region. Here we can immediately see from Figure 4 that the shape and magnitude of the binary peak are changing as the scattered electron angle increases. For example, for a scattered electron angle of $-7.5°$, the maximum intensity of the TDCS occurs close to the momentum transfer direction (+K). As θ_1 increases, we now see that the maximum intensity shifts away from the momentum transfer direction. Indeed, we also observe a local minimum in the vicinity of the momentum transfer direction for $\theta_1 = -15.0°$. This behaviour resembles that previously observed for the ionization of the unresolved 4a″ + 3a″ orbitals of phenol, under similar kinematical conditions.[39] The 4a″ and 3a″ orbitals of phenol are both out-of-plane ring bonding/O(2p) orbitals, which therefore resemble the $2b_{3u}$ and $1b_{1g}$ orbitals of pBQ. This raises the intriguing possibility that out-of-plane ring bonding/O(2p) orbitals may possess a characteristic TDCS angular distribution, although further work to confirm this is clearly needed.

We now compare the present experimental data to our theoretical calculations (see Figure 4). The M3DW calculation produces an angular distribution that has a peak in the binary direction that is similar to that observed in the experimental profile for the scattered electron angle of $-7.5°$, although the theoretical distribution does not exhibit the particularly broad nature of the binary lobe seen experimentally at the larger ejected electron angles, $\theta_2 = 90°$-$120°$. As the scattered electron angle increases the agreement between the shape of the TDCS in the binary region for the experimental data and that predicted by the M3DW calculation worsens. Specifically, while the M3DW TDCS calculations at larger scattering angles show a principal maximum in the momentum transfer direction, this is not seen experimentally. Regarding the absolute scale, the theoretical TDCS predicts an intensity in the binary region that increases as the scattered electron angle increases. This behaviour is consistent with the experimental observation from $\theta_1 = -7.5°$ to $-10.0°$, where the absolute intensity of the TDCS in the binary region is also seen to increase. However, differences exist in the absolute intensity behaviour between theory and experiment, with the experimental TDCS reaching its maximum TDCS intensity at $\theta_1 = -10.0°$ before it decreases as the scattered electron angle increases to $-15.0°$, while the intensity of the M3DW binary region TDCS continues to increase as the scattered electron angle becomes larger. We note that this behaviour of the M3DW cross sections was also observed in our study on furfural.[38] In terms of the DWBA calculations, we found that these give TDCS angular distributions that are very similar to those calculated using the M3DW method at each θ_1, although the DWBA calculations gave a slightly larger absolute value for the TDCS across most angular regions for each scattering angle. Finally, we highlight the significant variation in the absolute scale of the TDCS as the scattered electron angle varies. This result illustrates the importance of obtaining absolute experimental cross section data in order

to provide a full assessment of the validity of the theoretical calculations.

As neither of the M3DW or DWBA methods were able to quantitatively reproduce the experimental results, we are interested to try and qualitatively explain the experimental observations with a view to improving the theoretical description of the electron impact ionization dynamics of complex molecules. To this end, we consider the relevant orbital momentum profiles of the ionized orbitals shown in Fig. 5. Our approach originates from electron momentum spectroscopy,[33–35] where the internal electronic structure of the target is probed through impulsive collisions at high-impact energies. Under the present asymmetric coplanar kinematic conditions at intermediate impact energies, the impulse approximation breaks down and the collisional and structural components become intertwined. However, consideration of the momentum profiles within an impulse approximation (the momentum of the ionized target's electron is equal in magnitude but opposite in sign to the ion recoil momentum) may provide some qualitative explanation of the present observed TDCS.[39,41,57] In this context, the range of possible recoil momentum values available to conserve momentum is also shown in Fig. 5 for each experimental scattered electron angle considered. Here the recoil momentum of the ion is at its minimum, q_{min}, in the direction of the momentum transfer (+K), while it is at its maximum, q_{max}, in the direction anti-parallel to the momentum transfer (−K); see also Fig. 2(b).

From Figure 5 we can see that for a scattered electron angle of −7.5°, the momentum profile is at its maximum for the minimum magnitude of the recoil momentum, q_{min}. As the scattering angle increases, the range of possible recoil momentum values increases and it becomes possible to sample different sections of the momentum profile. Specifically, the intensity of the orbital momentum profile sampled in the momentum transfer direction (+K) decreases, which in turn results in a local minimum in this direction. The maximum in the momentum profile is then located away from the momentum transfer directions and gives rise to the lobe structures observed in the TDCS, with these becoming more pronounced as the scattered electron angle increases. This interpretation thus qualitatively provides some explanation of the experimentally observed phenomena. It also suggests that one possible issue with the current theoretical methods involves the spherically averaging approximations used in the calculations. Both the molecular orbital used for the bound state wavefunction and the distorting potential used to calculate the continuum electron wavefunctions are averaged over all orientations so the lack of agreement between theory and experiment might indicate strong orientation dependent effects.

We finally consider the behaviour of the triple differential cross sections for the electron impact ionization of the unresolved combination of the $4b_{3g} + 5b_{2u} + 1b_{1g} + 2b_{3u}$ orbitals within the recoil region (see Fig. 4). Experimentally, no significant intensity is observed in the recoil region for any of the scattered electron angles considered. From the theoretical perspective, both the M3DW and DWBA calculations also indicate weak recoil peak intensities. The absence of significant recoil intensity in pBQ under the current kinematical conditions is not particularly surprising. Previously we have investigated the (e,2e) TDCS for the 4a″ and 3a″ orbitals of phenol under comparable conditions[39] and similar to the current study these did not possess any significant recoil peak intensity. The 4a″ and 3a″ orbitals of phenol are both out-of-plane ring bonding/O(2p) orbitals, which therefore resemble the $2b_{3u}$ and $1b_{1g}$ orbitals of pBQ investigated as a part of this work. The absence of significant recoil structure in phenol was attributed to the delocalisation of the electron density over the molecule, thus weakening any electron-nuclei scattering that is generally required to produce a significant recoil peak intensity. We believe that this is also likely to be the case for pBQ. This is supported by the M3DW calculations, where for both pBQ and phenol the out of plane orbitals have negligible recoil intensity under the present kinematical conditions. We also note that the behaviour of the angular distributions of the TDCS in the binary regions for pBQ and phenol show strong similarities, adding further support to our explanation. Correspondingly, this observation supports our assertion regarding the similarity observed in the binary peak region for pBQ and phenol, hence, that the ionization dynamics for similar types of molecular orbitals may possess a characteristic TDCS angular distribution profile.

Lastly, we reflect that the lack of recoil region intensity for pBQ suggests that the ionization model employed within the LEPTS framework[47–50] may be a good first approximation for describing electron transport through pBQ. However, as the sensitivity requirements on charged-particle track simulations improve, it appears that ionization treatment must be expanded to consider scattering processes where the secondary electron is ejected at angles away from the momentum transfer direction. This is especially true for larger momentum transfer collisions, where the maximum of the TDCS angular distribution does not often lie on the momentum transfer direction. However, until theoretical methods are developed that can robustly describe/explain scattering phenomena for complex molecular targets over a range of kinematical regimes, the ionization model described within the LEPTS framework appears reasonable. However, it is highly desirable to develop robust, theoretical description of the ionization behaviour of complex molecules as this will ultimately improve the quality of charged-particle track simulations.

IV. CONCLUSION

Experimental triple differential cross sections for the unresolved combination of the four outermost orbitals of *para*-benzoquinone were presented. These cross sections were experimentally inter-normalised to enable in-depth evaluation of the angular distribution and an absolute scale for comparison with predictions using different theoretical models. Unfortunately, our theoretical calculations, performed at the molecular 3-body distorted wave and distorted wave Born approximation levels of theory, were unable to quantitatively describe the observed behaviour of the TDCSs. Nonetheless, by considering the orbital momentum profiles of the ionized orbitals, we were able to provide a qualitative description of the experimentally observed phenomena. The

results presented in Figure 4 highlight the need for developing tractable theoretical scattering calculations that can adequately describe the molecular targets valence electronic structure. Finally, our systematic investigation into the ionization dynamics of this and similar molecules suggested that certain molecular orbitals may exhibit characteristic TDCS angular distributions.

ACKNOWLEDGMENTS

One of us (M.J.B.) acknowledges the Australian Research Council for some financial support. C.G.N. acknowledges the support from the National Natural Science Foundation of China (NSFC) (Grant No. 11174175). Computational work was carried out using LANL Institutional Computing Resources. The Los Alamos National Laboratory is operated by Los Alamos National Security, LLC for the National Nuclear Security Administration of the U.S. Department of Energy under Contract No. DE-AC5206NA25396. This work was partly supported by the US National Science Foundation under Grant. No. PHY-1505819 (EA and DM).

[1]A. Zouni, H.-T. Witt, J. Kern, P. Fromme, N. Krauss, W. Saenger, and P. Orth, Nature **409**, 739 (2001).
[2]A. J. Ragauskas, C. K. Williams, B. H. Davison, G. Britovsek, J. Cairney, C. A. Eckert, W. J. Frederick, J. P. Hallett, D. J. Leak, C. L. Liotta, J. R. Mielenz, R. Murphy, R. Templer, and T. Tschaplinski, Science **311**, 484 (2006).
[3]M. Hambourger, G. F. Moore, D. M. Kramer, D. Gust, A. L. Moore, and T. A. Moore, Chem. Soc. Rev. **38**, 25 (2009).
[4]O. Yehezkeli, R. Tel-Vered, J. Wasserman, A. Trifonov, D. Michaeli, R. Nechushtai, and I. Willner, Nat. Commun. **3**, 742 (2012).
[5]B. Huskinson, M. P. Marshak, C. Suh, S. Er, M. R. Gerhardt, C. J. Galvin, X. Chen, A. Aspuru-Guzik, R. G. Gordon, and M. J. Aziz, Nature **505**, 195 (2014).
[6]Y. Ding and G. Yu, Angew. Chem., Int. Ed. **55**, 4772 (2016).
[7]Y. Honda, M. Hada, M. Ehara, and H. Nakatsuji, J. Phys. Chem. A **106**, 3838 (2002).
[8]G. Ter Horst and J. Kommandeur, Chem. Phys. **44**, 287 (1979).
[9]R. Pou-Amérigo, M. Merchán, and E. Ortí, J. Chem. Phys. **110**, 9536 (1999).
[10]J. Weber, K. Malsch, and G. Hohlneicher, Chem. Phys. **264**, 275 (2001).
[11]S. Knippenberg and M. S. Deleuze, J. Electron Spectrosc. Relat. Phenom. **178–179**, 61 (2010).
[12]T. N. V. Karsili, D. Tuna, J. Ehrmaier, and W. Domcke, Phys. Chem. Chem. Phys. **17**, 32183 (2015).
[13]P. Brint, J.-P. Connerade, P. Tsekeris, A. Bolovinos, and A. Baig, J. Chem. Soc., Faraday Trans. 2 **82**, 367 (1986).
[14]D. A. Horke, Q. Li, L. Blancafort, and J. R. R. Verlet, Nat. Chem. **5**, 711 (2013).
[15]T. M. Dunn and A. H. Francis, J. Mol. Spectrosc. **50**, 14 (1974).
[16]J. M. Hollas, Spectrochim. Acta **20**, 1563 (1964).
[17]T. Itoh, Chem. Rev. **95**, 2351 (1995).
[18]B. Ómarsson and O. Ingólfsson, Phys. Chem. Chem. Phys. **15**, 16758 (2013).
[19]M. Allan, Chem. Phys. **84**, 311 (1984).
[20]L. G. Christophorou, J. G. Carter, and A. A. Christodoulides, Chem. Phys. Lett. **3**, 237 (1969).
[21]P. M. Collins, L. G. Christophorou, E. L. Chaney, and J. G. Carter, Chem. Phys. Lett. **4**, 646 (1970).
[22]C. D. Cooper, W. T. Naff, and R. N. Compton, J. Chem. Phys. **63**, 2752 (1975).
[23]M. Allan, Chem. Phys. **81**, 235 (1983).
[24]S. A. Pshenichnyuk, N. L. Asfandiarov, V. S. Fal'ko, and V. G. Lukin, Int. J. Mass Spectrom. **227**, 281 (2003).
[25]C. W. West, J. N. Bull, E. Antonkov, and J. R. R. Verlet, J. Phys. Chem. A **118**, 11346 (2014).
[26]O. G. Khvostenko, P. V. Shchukin, G. M. Tuimedov, M. V. Muftakhov, E. E. Tseplin, S. N. Tseplina, and V. A. Mazunov, Int. J. Mass Spectrom. **273**, 69 (2008).
[27]D. Dougherty and S. P. McGlynn, J. Am. Chem. Soc. **99**, 3234 (1977).
[28]J. F. Stanton, K. W. Sattelmeyer, J. Gauss, M. Allan, T. Skalicky, and T. Bally, J. Chem. Phys. **115**, 1 (2001).
[29]C. R. Brundle, M. B. Robin, and N. A. Kuebler, J. Am. Chem. Soc. **94**, 1466 (1972).
[30]L. Åsbrink, G. Bieri, C. Fridh, E. Lindholm, and D. P. Chong, Chem. Phys. **43**, 189 (1979).
[31]N. Kishimoto, K. Okamura, and K. Ohno, J. Chem. Phys. **120**, 11062 (2004).
[32]K. Piech, T. Bally, T. Ichino, and J. Stanton, Phys. Chem. Chem. Phys. **16**, 2011 (2014).
[33]E. Weigold and I. E. McCarthy, *Electron Momentum Spectroscopy* (Kluwer Academic/Plenum Publishers, New York, 1999).
[34]M. J. Brunger and W. Adcock, J. Chem. Soc. Perkin Trans. 2 **2002**, 1 (2002).
[35]M. Takahashi, Bull. Chem. Soc. Jpn. **82**, 751 (2009).
[36]A. Lahmam-Bennani, J. Electron Spectrosc, Relat. Phenom. **123**, 365 (2002).
[37]J. D. Builth-Williams, S. M. Bellm, D. B. Jones, H. Chaluvadi, D. H. Madison, C. G. Ning, B. Lohmann, and M. J. Brunger, J. Chem. Phys. **136**, 024304 (2012).
[38]D. B. Jones, E. Ali, K. L. Nixon, P. Limão-Vieira, M.-J. Hubin-Franskin, J. Delwiche, C. G. Ning, J. Colgan, A. J. Murray, D. H. Madison, and M. J. Brunger, J. Chem. Phys. **143**, 184310 (2015).
[39]G. B. da Silva, R. F. C. Neves, L. Chiari, D. B. Jones, E. Ali, D. H. Madison, C. G. Ning, K. L. Nixon, M. C. A. Lopes, and M. J. Brunger, J. Chem. Phys. **141**, 124307 (2014).
[40]J. D. Builth-Williams, G. B. da Silva, L. Chiari, D. B. Jones, H. Chaluvadi, D. H. Madison, and M. J. Brunger, J. Chem. Phys. **140**, 214312 (2014).
[41]D. B. Jones, J. D. Builth-Williams, S. M. Bellm, L. Chiari, H. Chaluvadi, D. H. Madison, C. G. Ning, B. Lohmann, O. Ingolfsson, and M. J. Brunger, Chem. Phys. Lett. **572**, 32 (2013).
[42]J. D. Builth-Williams, S. M. Bellm, L. Chiari, P. A. Thorn, D. B. Jones, H. Chaluvadi, D. H. Madison, C. G. Ning, B. Lohmann, G. B. da Silva, and M. J. Brunger, J. Chem. Phys. **139**, 034306 (2013).
[43]S. M. Bellm, J. D. Builth-Williams, D. B. Jones, H. Chaluvadi, D. H. Madison, C. G. Ning, F. Wang, X. G. Ma, B. Lohmann, and M. J. Brunger, J. Chem. Phys. **136**, 244301 (2012).
[44]O. Zatsarinny and K. Bartschat, Phys. Rev. A **85**, 032708 (2012).
[45]X. Ren, A. Senftleben, T. Pflüger, A. Dorn, K. Bartschat, and J. Ullrich, Phys. Rev. A **83**, 052714 (2011).
[46]M. Ulu, Z. N. Ozer, M. Yavuz, O. Zatsarinny, K. Bartschat, M. Dogan, and A. Crowe, J. Phys. B: At., Mol. Opt. Phys. **46**, 115204 (2013).
[47]A. G. Sanz, M. C. Fuss, A. Muñoz, F. Blanco, P. Limão-Vieira, M. J. Brunger, S. J. Buckman, and G. García, Int. J. Radiat. Biol. **88**, 71 (2012).
[48]M. C. Fuss, A. G. Sanz, A. Muñoz, F. Blanco, M. J. Brunger, S. J. Buckman, P. Limão-Vieira, and G. García, Appl. Radiat. Isot. **83**, 159 (2014).
[49]M. C. Fuss, L. Ellis-Gibbings, D. B. Jones, M. J. Brunger, F. Blanco, A. Muñoz, P. Limão-Vieira, and G. García, J. Appl. Phys. **117**, 214701 (2015).
[50]M. J. Brunger, K. Ratnavelu, S. J. Buckman, D. B. Jones, A. Muñoz, F. Blanco, and G. García, Eur. Phys. J. D **70**, 46 (2016).
[51]F. Blanco, A. Muñoz, D. Almeida, F. Ferreira da Silva, P. Limão-Vieira, M. C. Fuss, A. G. Sanz, and G. García, Eur. Phys. J. D **67**, 199 (2013).
[52]S. J. Cavanagh and B. Lohmann, J. Phys. B: At., Mol. Opt. Phys. **32**, L261 (1999).
[53]M. J. Frisch, G. W. Trucks, H. B. Schlegel, G. E. Scuseria, M. A. Robb, J. R. Cheeseman, G. Scalmani, V. Barone, B. Mennucci, G. A. Petersson, H. Nakatsuji, M. Caricato, X. Li, H. P. Hratchian, A. F. Izmaylov, J. Bloino, G. Zheng, J. L. Sonnenberg, M. Hada, M. Ehara, K. Toyota, R. Fukuda, J. Hasegawa, M. Ishida, T. Nakajima, Y. Honda, O. Kitao, H. Nakai, T. Vreven, J. A. Montgomery, J. E. Peralta, F. Ogliaro, M. Bearpark, J. J. Heyd, E. Brothers, K. N. Kudin, V. N. Staroverov, R. Kobayashi, J. Normand, K. Raghavachari, A. Rendell, J. C. Burant, S. S. Iyengar, J. Tomasi, M. Cossi, N. Rega, J. M. Millam, M. Klene, J. E. Knox, J. B. Cross, V. Bakken, C. Adamo, J. Jaramillo, R. Gomperts, R. E. Stratmann, O. Yazyev, A. J. Austin, R. Cammi, C. Pomelli, J. W. Ochterski, R. L. Martin, K. Morokuma, V. G. Zakrzewski, G. A. Voth, P. Salvador, J. J. Dannenberg, S. Dapprich, A. D. Daniels, Ö. Farkas, J. B. Foresman, J. V. Ortiz, J. Cioslowski, and D. J. Fox, GAUSSIAN 09, Revision B.01, Gaussian, Inc. 2010.
[54]J. P. D. Cook and C. E. Brion, Chem. Phys. **69**, 339 (1982).
[55]D. H. Madison and O. Al-Hagan, J. At., Mol., Opt. Phys. **2010**, 367180.
[56]J. Gao, J. L. Peacher, and D. H. Madison, J. Chem. Phys. **123**, 204302 (2005).
[57]S. Xu, X. Ma, S. Yan, and P. Zhang, J. Chem. Phys. **136**, 237101 (2012).